Interaction of ^{8}He with ^{208}Pb at near-barrier energies: ^{4}He and ^{6}He production

G. Marquínez-Durán,[1] I. Martel,[1] A. M. Sánchez-Benítez,[2] L. Acosta,[3] J. L. Aguado,[1] R. Berjillos,[1] A. R. Pinto,[1] T. García,[1]
J. A. Dueñas,[4] K. Rusek,[5] N. Keeley,[6,*] K. W. Kemper,[7,5] M. A. G. Álvarez,[8] M. J. G. Borge,[9] A. Chbihi,[10] C. Cruz,[9]
M. Cubero,[11,12,9] J. P. Fernández-García,[8] B. Fernández-Martínez,[13] J. L. Flores,[14] J. Gómez-Camacho,[13,8] J. A. Labrador,[13]
F. M. Marqués,[15] A. M. Moro,[8] M. Mazzocco,[16] A. Pakou,[17] V. V. Parkar,[1,†] N. Patronis,[17] V. Pesudo,[9] D. Pierroutsakou,[18]
R. Raabe,[19] R. Silvestri,[18] N. Soić,[20] Ł. Standyło,[5] I. Strojek,[6] O. Tengblad,[9] R. Wolski,[21,22] and Z. Abou-Haidar[13]

[1]*Science and Technology Research Centre (STRC), University of Huelva, 21071 Huelva, Spain*
[2]*Departamento de Ciencias Integradas y Centro de Estudios Avanzados en Física, Matemáticas y Computación,*
Facultad de Ciencias Experimentales, Universidad de Huelva, 21071 Huelva, Spain
[3]*Instituto de Física, Universidad Nacional Autónoma de México, A.P. 20-364, Distrito Federal 01000, Mexico*
[4]*Departamento Ingeniería Eléctrica y Centro de Estudios Avanzados en Física, Matemáticas y Computación,*
Universidad de Huelva, 21071 Huelva, Spain
[5]*Heavy Ion Laboratory, University of Warsaw, ul. Pasteura 5a, 02-093 Warsaw, Poland*
[6]*National Centre for Nuclear Research, ul. Andrzeja Sołtana 7, 05-400 Otwock, Poland*
[7]*Department of Physics, Florida State University, Tallahassee, Florida 32306, USA*
[8]*Departamento de Física Atómica, Molecular y Nuclear, Universidad de Sevilla, 41080 Seville, Spain*
[9]*Instituto de Estructura de la Materia, CSIC, 28006 Madrid, Spain*
[10]*GANIL, CEA and IN2P3-CNRS, B.P. 5027, 14076 Caen Cedex, France*
[11]*Escuela de Física, Universidad de Costa Rica, 11501 apdo. 2060 San José, Costa Rica*
[12]*CICANUM, Universidad de Costa Rica, 11502 apdo. 2060 San José, Costa Rica*
[13]*Centro Nacional de Aceleradores (Universidad de Sevilla, Junta de Andalucía, CSIC), 41092 Seville, Spain*
[14]*Departamento de Ingeniería Eléctrica, Universidad de Huelva, 21071 Huelva, Spain*
[15]*Laboratoire de Physique Corpusculaire, 14050 Caen Cedex, France*
[16]*Dipartimento di Fisica and INFN, Università di Padova, 35131 Padova, Italy*
[17]*Department of Physics and HINP, University of Ioannina, 45110 Ioannina, Greece*
[18]*INFN - Sezione di Napoli, Via Cintia, 80126 Napoli, Italy*
[19]*KU Leuven, Intituut voor Kern-en Stralingsfysica, Celestijnenlaan 200D, 3001 Leuven, Belgium*
[20]*Rudjer Bošković Institute, Bijenicka 54, 10000 Zagreb, Croatia*
[21]*Institute of Nuclear Physics PAN, Kraków, Poland*
[22]*Flerov Laboratory of Nuclear Reactions, JINR, Dubna 141980, Russia*

Angular distributions for the inclusive ^{4}He and ^{6}He production cross sections in the ^{8}He + ^{208}Pb system at incident energies of 16 and 22 MeV measured at the SPIRAL facility of the GANIL laboratory are presented. Using a combination of kinematical arguments and distorted wave Born approximation (DWBA) calculations, neutron transfer reactions were inferred to be the dominant contributors to both inclusive cross sections. Model-dependent values for the ratios of two- to one-neutron stripping, σ_{2n}/σ_{1n}, were derived and compared with previous results for ^{8}He and ^{6}He projectiles incident on other heavy targets. Three- and four-neutron stripping were inferred to be the main processes leading to ^{4}He production, although the exact mechanism remains to be elucidated.

I. INTRODUCTION

Recently, precise data for the elastic scattering of ^{8}He from a ^{208}Pb target at an incident energy of 22 MeV, slightly above the Coulomb barrier, were presented and compared with existing data for ^{6}He + ^{208}Pb at the same incident energy [1]. A larger total reaction cross section was obtained for ^{8}He than for ^{6}He, suggesting an increased neutron stripping cross section for ^{8}He that more than compensates for an expected lower breakup cross section than ^{6}He, due to its higher breakup threshold and probable weaker dipole coupling to the continuum.

Some experimental studies of the reactions of ^{8}He incident on heavy targets at near-barrier energies have already been performed. Direct and fusion-evaporation reactions for the ^{8}He + ^{208}Pb system were studied at 26 MeV via γ spectroscopy [2]. Although the statistics were low, the

---

observed population of low-spin states in ^{209}Pb suggests a strong $1n$ stripping process, with a cross section comparable to that for the most probable fusion-evaporation channel, ^{208}Pb(^{8}He, $4n$)^{212}Po, to within a factor of about 2 in favor of fusion evaporation. In Refs. [3,4], measurements of heavy residue production in the ^{8}He $+$ ^{197}Au system at several near-barrier energies are presented. Excitation functions are reported which show that neutron stripping dominates over fusion for energies up to about 10 MeV above the barrier. Coupled reaction channels (CRC) calculations that describe the total neutron transfer strength provide a good simultaneous description of the fusion excitation function, suggesting that breakup is not as important for ^{8}He as for ^{6}He. A comparison between the fusion cross sections (σ_{Fus}) for the ^{4,6,8}He $+$ ^{197}Au systems showed that σ_{Fus} for ^{6}He and ^{8}He are similar at energies below the barrier and larger than for ^{4}He.

In this work, we present inclusive ^{4}He and ^{6}He production angular distributions for the ^{8}He $+$ ^{208}Pb system at incident energies of 16 and 22 MeV. A combination of kinematics and calculations enables a number of conclusions to be drawn concerning the relative importance of neutron stripping reactions, as well as an upper limit on the fusion cross section at 22 MeV.

II. EXPERIMENT AND DATA ANALYSIS

The experiment was carried out at the SPIRAL facility of the GANIL laboratory in Caen, France, and a detailed description of the experimental setup was given in Refs. [1,5]. As shown in these works, the double-sided silicon strip detector ΔE-E telescopes of the GLORIA array [5] provided clear separation between the He isotopes produced in the interaction between the beam and target so that the ^{8}He, ^{6}He, and ^{4}He yields were unambiguously extracted. The strip detectors are subdivided into pixels, defined as the intersection of a p strip (vertical) and an n strip (horizontal), see Ref. [5], with each pixel covering 3–4° in the laboratory frame at the target. The ΔE and E stages of the telescopes were 40 μm and 1 mm thick, respectively. The rapid variation of the elastic scattering as a function of scattering angle required great care in determining the angle of each pixel since, as usual with radioactive beams, the beam spot on target was large, $\sim$3.5 mm in diameter. The procedure for establishing the detection angle of a given strip is given in Ref. [1] and relied on comparing a detailed simulation of the detection system with the elastic scattering in the region where it is dominated by Coulomb scattering.

In addition to the previously reported elastic scattering data at a ^{8}He incident energy of 22 MeV [1], elastic scattering data were also obtained at 16 MeV and ^{6}He and ^{4}He yields at both energies. Figure 1(a) shows the events from all the strip detectors gated on ^{4}He at 22 MeV. The vertical axis is the total energy deposited in a given telescope as a function of the scattering angle. The intense horizontal line at the bottom of the figure corresponds to α particles arising from fusion-evaporation events, matching very well the α-decay energies of ^{212}Po. There are two other main groups, the first at scattering angles between 60 and 160° from neutron transfer reactions and a second, weaker group at forward angles, between 20 and 40°, from ^{8}He $\rightarrow$ ^{4}He $+$ $4n$ breakup.

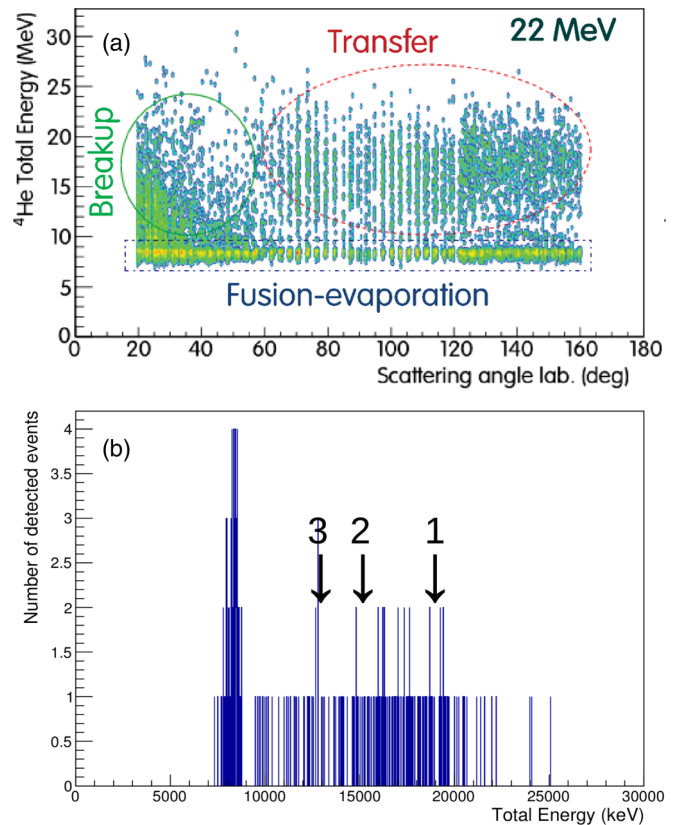
FIG. 1. (a) Total energy vs scattering angle for events gated on ^{4}He produced in the ^{8}He $+$ ^{208}Pb interaction at an incident energy of 22 MeV. Regions corresponding to the different production mechanisms are labeled. (b) Number of counts vs energy for events gated on ^{4}He summed over pixels at a scattering angle of $\theta_{\mathrm{lab}} = 94.5°$. The numbered arrows denote the energy of ^{4}He ejectiles corresponding to the optimum Q values of Table II for the following reactions: (1) ^{208}Pb(^{8}He, ^{4}He)^{212}Pb, (2) ^{208}Pb(^{8}He, ^{5}He $\rightarrow$ ^{4}He $+$ n)^{211}Pb, and (3) ^{208}Pb(^{8}He, ^{6}He$^*_{1.8}$ $\rightarrow$ ^{4}He $+$ $2n$)^{210}Pb. For reactions 2 and 3, the arrows mark the centers of the energy distributions of ^{4}He arising from the decay of the ^{5}He $3/2^-$ ground-state resonance and the ^{6}He 1.8-MeV 2^+ resonance, respectively; see text for further details. The narrow peak at approximately 8.8 MeV corresponds to α particles from the decay of the ground state of ^{212}Po produced by fusion evaporation.

These regions are drawn following many published heavy-ion reaction data, where it is always found that for energies below the Coulomb barrier the transfer cross section peaks at 180° and falls off more or less rapidly as the scattering angle decreases until it becomes negligible at forward angles. For incident energies just above the Coulomb barrier, the transfer angular distributions exhibit the classical bell-shaped peak structure, with the peak angle gradually moving to more forward angles as the incident energy increases. Both incident energies studied in this experiment were sufficiently low that there was a clear kinematic separation between transfer and breakup and any ^{4}He and ^{6}He events at forward angles necessarily arise from breakup processes since the transfer cross sections will be negligible in this region. There may be some slight overlap of breakup and transfer contributions
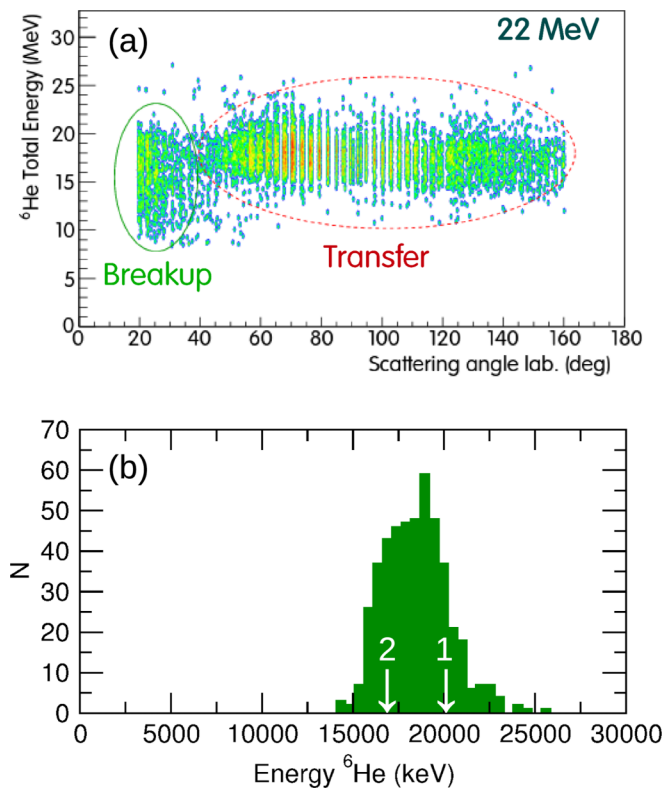
FIG. 2. (a) Total energy vs scattering angle for events gated on ^{6}He produced in the ^{8}He + ^{208}Pb interaction at an incident energy of 22 MeV. Regions corresponding to the different production mechanisms are labeled. (b) Number of counts vs energy for events gated on ^{6}He summed over pixels at a scattering angle of $\theta_{\text{lab}} = 70°$. The numbered arrows denote the energy of ^{6}He ejectiles corresponding to the optimum Q values of Table II for the following reactions: (1) ^{208}Pb(^{8}He, ^{6}He)^{210}Pb and (2) ^{208}Pb(^{8}He, ^{7}He $\rightarrow$ ^{6}He + n)^{209}Pb. For reaction 2, the arrow marks the center of the energy distribution of ^{6}He arising from the decay of the ^{7}He $3/2^-$ ground-state resonance; see text for further details.

but this is not expected to be significant. The shapes of the extracted inclusive angular distributions and distorted wave Born approximation (DWBA) calculations provide *a posteriori* justification for these conclusions. The energy spectrum of events gated on ^{4}He from several pixels around $\theta_{\text{lab}} = 94.5°$ added together is given in Fig. 1(b). In Fig. 2, we show similar plots for events gated on ^{6}He.

In Fig. 3, we present the elastic scattering data for an incident ^{8}He energy of 16 MeV, together with the previously published data at 22 MeV [1]. The solid curves represent optical model fits to the data. The 22-MeV curve employs the potential parameters from Table I of Ref. [6]. These also give a reasonable description of the data at 16 MeV but the best fit, displayed on Fig. 3 as the solid red curve, was obtained by increasing the imaginary well depth W to 50.0 MeV. The dashed red curve denotes the 16-MeV elastic scattering angular distribution calculated using the same optical potential parameters as at 22 MeV. There is a small but noticeable difference in the angular distribution calculated with these parameters compared to the best fit,
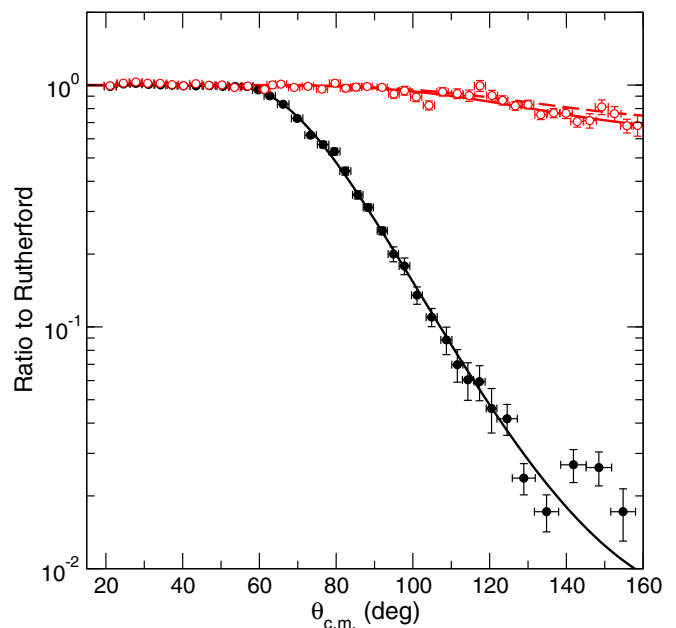

FIG. 3. Angular distributions for the ^{8}He + ^{208}Pb elastic scattering at 16 MeV (open circles) and 22 MeV [1] (filled circles). The solid curves denote optical model fits to the data; see text for details. The dashed curve denotes the 16-MeV elastic scattering angular distribution calculated using the same optical potential parameters as at 22 MeV.

leading to an $\sim$8% increase in χ^2 and a $\sim$24% decrease in total reaction cross section (σ_R) compared to the best-fit values. The σ_R extracted from the optical model fits are given in Table I. The uncertainties represent the effect of varying W such that χ^2 increased by 10% compared to the minimum values.

Ratios of the number of ^{6}He to ^{8}He and ^{4}He to ^{8}He detected, the latter excluding the ^{4}He at low energies arising from fusion evaporation, were formed for each pixel and the results converted into laboratory frame absolute cross sections by multiplying by the appropriate elastic scattering cross-section angular distributions obtained from the optical model fits to the elastic scattering data, suitably transformed to the laboratory frame. The resulting angular distributions are plotted in Fig. 4. Errors are purely statistical. It is apparent that

TABLE I. Integrated cross sections for ^{6}He ($\sigma_{^6\text{He}}$) and ^{4}He ($\sigma_{^4\text{He}}$) production obtained from fits to the experimental angular distributions shown in Fig. 4. Also given are the total reaction cross sections from the optical model fits to the elastic scattering data plotted on Fig. 3 (σ_R) and total $1n$-stripping cross sections (σ_{1n}) from the DWBA calculations described in Sec. III, while $\sigma_{\text{Fus}} = \sigma_R - (\sigma_{^6\text{He}} + \sigma_{^4\text{He}})$ represents an upper limit on the fusion cross section.

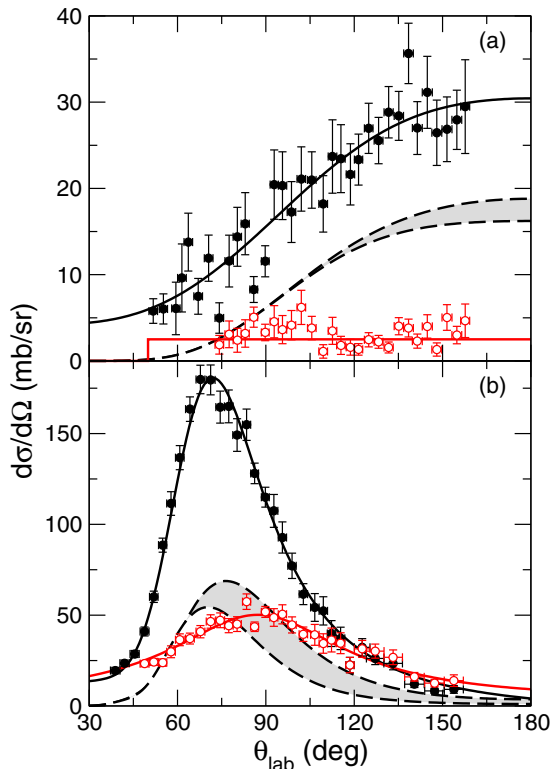| E_{lab} (MeV)	σ_{1n} (mb)	$\sigma_{^6\text{He}}$ (mb)	$\sigma_{^4\text{He}}$ (mb)	σ_R (mb)	σ_{Fus} (mb)
16	90 ± 3	203^{+10}_{-28}	26 ± 5	254 ± 60	25^{+61}_{-66}
22	292 ± 61	871 ± 31	393^{+10}_{-33}	1529 ± 40	265^{+52}_{-60}

FIG. 4. Laboratory frame angular distributions of total ^{6}He (filled circles) and ^{4}He (open circles) yields at 16 (a) and 22 MeV (b). The solid curves represent fits to the data while the dashed curves and gray shaded areas denote the results of ^{208}Pb(^{8}He, ^{7}He)^{209}Pb single-neutron stripping DWBA calculations including the uncertainties due to the use of different distorting potentials in the exit channels (see text for details).

the shapes of the angular distributions (with the exception of the ^{4}He yield at 16 MeV where the statistics are too low to determine accurately the shape) are characteristic of transfer reactions. However, it will be noted that the angular distributions displayed in Fig. 4 are confined to angles $\theta_{lab} > \sim 40°$ whereas the measurements extend down to $\theta_{lab} = 20°$, as seen in Figs. 1 and 2. This cutoff was imposed by the angular resolution of the pixels of the GLORIA array. At forward angles (in this case, for angles $\theta_{lab} \lesssim 40°$) the elastic scattering cross section varies too rapidly as a function of angle over the range subtended by a pixel for a reliable absolute cross section to be extracted from the ^{6}He to ^{8}He and ^{4}He to ^{8}He ratios (the ratios themselves are, of course, unaffected by this problem). At larger angles, the variation of the elastic scattering cross section as a function of angle is slow enough not to cause a problem. This does mean that we are, unfortunately, unable to make any quantitative deductions concerning the contribution of breakup to the ^{6}He and ^{4}He yields.

The solid curves on Fig. 4 represent fits to the experimental angular distributions. At 16 MeV, the ^{6}He yield was fitted with a third-order Legendre polynomial which reproduces the shape very well. The ^{4}He yield was simply fitted by two straight line segments, 0 mb/sr for angles $0° < \theta_{lab} < 50°$ and 2.5 mb/sr for $50° < \theta_{lab} < 180°$. At 22 MeV, the ^{6}He yield

was well reproduced by the sum of two Lorentzian peaks while the ^{4}He yield was well described by a single Lorentzian. The integrated cross sections obtained from these fits are given in Table I. The uncertainties were estimated by scaling the fits to give χ^2 values 20% greater than the minimum values. The asymmetric errors on some values reflect the scatter in the points, emphasized somewhat by this procedure.

III. DISCUSSION

In Tables II and III, we give the Q values for the various direct reaction processes that can yield ^{4}He and ^{6}He nuclei in the exit channel, respectively, together with the optimum Q values for the $A(a, b)B$ transfer processes calculated according to the Brink matching rules [7,8]:

$$Q_{opt} = (Z_b Z_B - Z_a Z_A)e^2/R - \frac{1}{2}mv^2, \qquad (1)$$

where the charge on nucleus i is denoted by $Z_i e$, the relative velocity of the two nuclei in the region of interaction (separated by distance R) by v, and the mass of the transferred particle by m. For transfers of neutron(s), the first term is zero so Q_{opt} will always be negative in these cases. The relative velocity v may be calculated as [9]

$$v = [2(E_{c.m.} - E_B)/\mu]^{1/2}, \qquad (2)$$

where E_B and μ are the Coulomb barrier and reduced mass of the projectile-target system, respectively. We took a Coulomb barrier of 18 MeV, similar to the empirical result of Ref. [10] for the ^{6}He $+$ ^{208}Pb system, when calculating the relative velocity of the ^{8}He $+$ ^{208}Pb nuclei. The Q_{opt} values given are for an incident ^{8}He energy of 22 MeV.

Tables II and III indicate that the ^{4}He production is the most complicated of the two, since more processes may, in principle, contribute. However, Fig. 1(a) suggests that the ^{4}He arising from breakup are well separated from those produced by transfer events. Three-body kinematics calculations with the code PAKINE3 [11] support this suggestion, indicating that at the angles where we have extracted the angular distributions the contribution to the ^{4}He yield from breakup should be negligible. The three numbered arrows on Fig. 1(b) mark the energies of ^{4}He ejectiles corresponding to Q_{opt} for the following reactions: (1) ^{208}Pb(^{8}He, ^{4}He)^{212}Pb, (2) ^{208}Pb(^{8}He, ^{5}He $\to$ ^{4}He $+$ n)^{211}Pb, and (3) ^{208}Pb(^{8}He, ^{6}He$^*_{1.8}$ $\to$ ^{4}He $+$ $2n$)^{210}Pb. For reactions 2 and 3, the markers are positioned at the centers of the range of allowed ^{4}He energies from the decay of the $3/2^-$ ground-state resonance of ^{5}He and the 1.8-MeV 2^+ resonance of ^{6}He, respectively, calculated with PAKINE3. These distributions are approximately ± 3.0 and ± 3.7 MeV wide, respectively. The possibility of Coulomb postacceleration was neglected. These kinematic considerations are consistent with the shape of the angular distribution in Fig. 4, indicating a dominant contribution from transfer reactions to the ^{4}He production mechanism.

We may make one further deduction concerning the ^{4}He production. Despite being the best matched of the three transfer processes that yield ^{4}He in the exit channel, the ^{208}Pb(^{8}He, ^{6}He$^*_{1.8}$ $\to$ ^{4}He $+$ $2n$)^{210}Pb reaction is unlikely to

TABLE II. Q values for the various processes that can lead to the production of ^{4}He nuclei in the interaction of a ^{8}He beam with a ^{208}Pb target. Optimum Q values, $Q_{\rm opt}$, calculated according to the Brink [7,8] matching rules are also given for the transfer reactions.

Reaction	Q (MeV)	$Q_{\rm opt}$ (MeV)
^{208}Pb(^{8}He, ^{4}He)^{212}Pb	+14.99	−1.7
^{208}Pb(^{8}He, ^{5}He → ^{4}He + n)^{211}Pb	+9.12	−1.2
^{208}Pb(^{8}He, ^{6}He$^*_{1.8}$ → ^{4}He + 2n)^{210}Pb	+5.20	−0.8
^{208}Pb(^{8}He, ^{8}He* → ^{4}He + 4n)^{208}Pb	−3.11	
^{208}Pb(^{8}He, ^{8}He* → (^{6}He$^*_{1.8}$ → ^{4}He + 2n) + 2n)^{208}Pb	−3.94	

contribute significantly due to the small spectroscopic factor for the $\langle ^8$He $| ^6$He$^*_{1.8} + 2n\rangle$ overlap [13]. Coupled channel Born approximation (CCBA) calculations including direct transfer to both the 0^+ ground state and 1.8-MeV 2^+ excited state of ^{6}He and the inelastic coupling between them bears this out, predicting negligible cross sections for hypothetical states in ^{210}Pb at excitation energies such that the reaction Q value is close to $Q_{\rm opt}$. We may thus infer that the main production mechanisms for ^{4}He are the 4n and 3n stripping reactions, preferentially populating states in the residual ^{212}Pb and ^{211}Pb nuclei at excitation energies centered at about 17 and 10 MeV, respectively. However, it is not possible to infer anything about the details of the mechanism, i.e., whether the reactions proceed as direct, one-step transfers or sequential transfer of, e.g., two dineutron-like clusters in the case of the 4n stripping.

For the ^{6}He production, Fig. 2(a) suggests that ^{6}He arising from breakup are also well separated from those produced by transfers, and three-body kinematics calculations again support this, indicating that any breakup contribution to the extracted ^{6}He angular distributions should be negligible, breakup being essentially confined to forward angles. The numbered arrows on Fig. 2(b) mark the energies of ^{6}He ejectiles corresponding to $Q_{\rm opt}$ for the following reactions: (1) ^{208}Pb(^{8}He, ^{6}He)^{210}Pb and (2) ^{208}Pb(^{8}He, ^{7}He → ^{6}He + n)^{209}Pb. For reaction 2, the marker is positioned at the center of the range of allowed ^{6}He energies from the decay of the ^{7}He $3/2^-$ ground-state resonance, again calculated with PAKINE3. The distribution is approximately ±2.0 MeV wide.

We can make some further deductions concerning the ^{6}He production, although these will necessarily be more or less model dependent. The 1n stripping can be calculated rather accurately using the DWBA since the necessary spectroscopic factors are known and the reaction is well Q matched and thus most likely to be a one-step transfer process. Such

TABLE III. Q values for the various processes that can lead to the production of ^{6}He nuclei in the interaction of a ^{8}He beam with a ^{208}Pb target. Optimum Q values, $Q_{\rm opt}$, calculated according to the Brink [7,8] matching rules are also given for the transfer reactions.

Reaction	Q (MeV)	$Q_{\rm opt}$ (MeV)
^{208}Pb(^{8}He, ^{6}He)^{210}Pb	+7.00	−0.8
^{208}Pb(^{8}He, ^{7}He → ^{6}He + n)^{209}Pb	+1.40	−0.4
^{208}Pb(^{8}He, ^{8}He* → ^{6}He + 2n)^{208}Pb	−2.14	

calculations were therefore performed using the code FRESCO [12], with $\langle ^8$He $| ^7$He + $n\rangle$ and $\langle ^{209}$Pb $| ^{208}$Pb + $n\rangle$ overlaps taken from Refs. [13] and [14], respectively. The following states in ^{209}Pb were included: 0.0 MeV $9/2^+$, 0.78 MeV $11/2^+$, 1.42 MeV $15/2^-$, 1.57 MeV $5/2^+$, 2.03 MeV $1/2^+$, 2.49 MeV $7/2^+$, and 2.54 MeV $3/2^+$. The entrance channel optical potentials were taken from Table I of Ref. [6], with the imaginary well depth at 16 MeV increased to 50 MeV, as described in Sec. II. Since the exit channel potential is unknown, involving as it does the unbound ^{7}He nucleus, the effect of employing several different choices was investigated: (1) the same parameters as in the entrance channel, (2) the global ^{6}Li parameters of Cook [15], (3) the global ^{7}Li parameters of Cook [15], and (4) the 16 and 22 MeV ^{6}He + ^{208}Pb parameters of Ref. [16] for the calculations at incident ^{8}He energies of 16 and 22 MeV, respectively.

It was found that the cross sections calculated using these exit channel potentials all lie between two extreme values at both energies, those calculated with the entrance channel parameters (the smallest) and those calculated with the global ^{6}Li parameters of Ref. [15] (the largest). The summed angular distributions for the calculations using these parameters, transformed into the laboratory reference frame, are plotted on Fig. 4 as the dashed lines with the gray areas denoting the degree of uncertainty. Note that the angular distributions are for the ^{7}He particle, although given the large difference in mass between the ^{6}He and neutron fragments produced by its decay the ^{6}He distribution should not differ significantly. Monte Carlo calculations of the ^{6}He angular distribution, similar to those performed in Ref. [17] for the single-neutron stripping and pickup reactions in the ^{7}Be + ^{58}Ni system, using the calculated ^{7}He angular distributions as input confirm this. The mean values of the summed integrated cross sections are given in Table I with uncertainties indicating the range covered by the use of the different exit channel potentials. We thus see that 44^{+3}_{-6}% and 33 ± 7% of the total ^{6}He production cross section may be attributed to 1n stripping at ^{8}He incident energies of 16 and 22 MeV, respectively, the proportion diminishing slightly (within the uncertainty) as the beam energy is increased above the Coulomb barrier. The remaining cross section must come almost exclusively from 2n stripping since, as Fig. 2(b) shows, breakup may be ruled out as a significant contributor on purely kinematic grounds.

It is also possible to estimate an upper limit for the total fusion cross section by subtracting the integrated ^{6}He and ^{4}He cross sections from the total reaction cross section extracted from the optical model fits to the elastic scattering angular
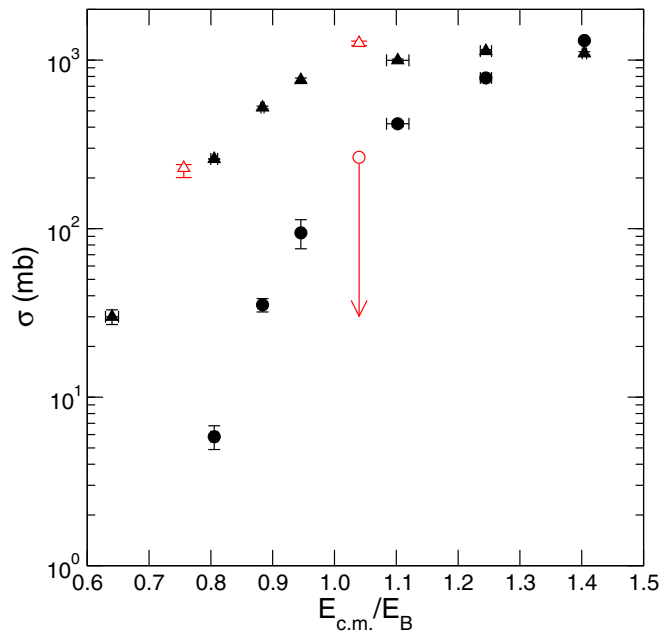
FIG. 5. Excitation functions of the fusion (filled circles) and neutron transfer (filled triangles) cross sections for the ^{8}He + ^{197}Au system [4] compared with the present results for the upper limit on fusion (open circle) and combined ^{4}He and ^{6}He cross sections (open triangles) for the ^{8}He + ^{208}Pb system.

distributions. Other contributions to the total reaction cross section should be small, DWBA estimates of the cross sections for inelastic scattering to the 2.60-MeV 3$^-$, 3.09-MeV 5$^-$, and 4.18-MeV 2$^+$ states of ^{208}Pb being negligible, for example. The resulting values are given in Table I. However, the uncertainty in the value at 16 MeV is such that we cannot make any meaningful deduction concerning the fusion cross section at this energy.

We may compare our results for the ^{8}He + ^{208}Pb system with those obtained by Lemasson *et al.* [3,4] for ^{8}He + ^{197}Au. The measured fusion and transfer excitation functions of Ref. [4] are plotted in Fig. 5, together with the upper limits on fusion and the sum of the ^{4}He and ^{6}He yields from this work as a function of $E_{\mathrm{c.m.}}/E_B$, where E_B is the nominal Coulomb barrier ($E_B = 19.84$ MeV for ^{8}He + ^{197}Au and $E_B = 20.37$ MeV for ^{8}He + ^{208}Pb). In this comparison, we have used the nominal barriers since only their difference (due to the different targets) is important here. The upper limit on the fusion cross section at 22 MeV is in good agreement with the data of Lemasson *et al.* [4]. The sum of the ^{4}He and ^{6}He production cross sections agrees reasonably well with the trend of the transfer cross-section data of Ref. [4], being approximately 25% larger at both 16 and 22 MeV. This could reflect a larger 1n-stripping cross section for the ^{208}Pb target due to the fragmentation of the single-neutron levels in ^{198}Au.

Lemasson *et al.* [3] also give model-independent lower limits on the ratio of 2n to 1n transfer cross sections, their only assumption being that any contributions to the observed ^{198}Au, ^{199}Au, and ^{198m}Au residue cross sections from 3n and 4n transfers could be neglected. We may carry out a similar exercise, although the result is necessarily model dependent

since it relies on the DWBA calculations for the 1n stripping cross sections. We further make the assumption, based on our inferences concerning the ^{4}He production, that 2n stripping only contributes significantly to the ^{6}He cross section so that $\sigma_{2n} = \sigma_{^6\mathrm{He}} - \sigma_{1n}$. We obtain values of $\sigma_{2n}/\sigma_{1n} = 1.26^{+0.12}_{-0.31}$ and 1.98 ± 0.48 at ^{8}He incident energies of 16 and 22 MeV, respectively, considerably larger than the results of Ref. [3] which range from about 0.1 to 0.3 but nevertheless compatible with them since they are *lower* limits. However, the rather large difference between our values and those of Lemasson *et al.* could indicate that either their assumption that contributions from 3n and 4n transfers could be neglected or our assumptions regarding 2n transfer require revision. Only full coincidence measurements, unfortunately not possible with currently available ^{8}He beam intensities, will be able to provide a definitive answer.

Our results for the σ_{2n}/σ_{1n} ratio may also be compared with similar values obtained with ^{6}He beams incident on heavy targets at energies close to the Coulomb barrier. A series of α-neutron coincidence measurements carried out at the TwinSol facility of the University of Notre Dame for the ^{6}He + ^{209}Bi system [18–20] gave a value of $\sigma_{2n}/\sigma_{1n} = 2.58 \pm 0.77$ for a beam energy of 22 MeV. Standyło *et al.* [21] obtained a value of about 1.4 for the same ratio in the ^{6}He + ^{206}Pb system at an incident ^{6}He energy of 18 MeV, although like the present result for ^{8}He + ^{208}Pb this is also model dependent. Both ^{6}He values are fully compatible with our ^{8}He results.

IV. CONCLUSIONS

The inclusive ^{4}He and ^{6}He yields were measured for the ^{8}He + ^{208}Pb system at ^{8}He incident energies of 16 and 22 MeV. Employing a combination of kinematics and model calculations it was possible to draw some model-dependent but nevertheless reasonably robust conclusions as to the production mechanisms. It is clear from the discussion in the previous section that breakup can only make a small contribution to the inclusive ^{4}He and ^{6}He cross sections in this system at near-barrier energies. First, any breakup events seem to be kinematically rather well separated from those due to transfer processes. Second, the shapes of the angular distributions (and their evolution with increasing beam energy) are consistent with those of transfer reactions. Finally, the upper limit on the fusion cross section at 22 MeV obtained by subtracting the integrated ^{4}He and ^{6}He cross sections from the total reaction cross section extracted from an optical model fit to the elastic scattering data leaves little or no room for a significant breakup cross section when compared to the measured fusion cross sections for the ^{8}He + ^{197}Au system [4].

The σ_{2n}/σ_{1n} ratios obtained from our analysis, while model dependent since they rely on calculated values for σ_{1n}, are compatible with the model-independent lower limits obtained by Lemasson *et al.* [3] for the ^{8}He + ^{197}Au system. They are also compatible with the results for the ^{6}He + ^{209}Bi [18–20] and ^{6}He + ^{206}Pb [21] systems. This is consistent with the intriguing possibility that the structure of ^{8}He may be represented as a ^{4}He core plus two dineutron-like clusters arranged on opposite sides of the core, somewhat similar to the model proposed by Nesterov *et al.* [22]. Given that the matching

conditions for $1n$ and $2n$ stripping are similar for ^{6}He and ^{8}He (they are somewhat better matched for ^{8}He) the cross sections should roughly scale according to the spectroscopic factors. In this simple picture, the spectroscopic factors for $1n$ and $2n$ stripping for ^{8}He would both be twice those for ^{6}He, since the probability of stripping either a single neutron or a dineutron-like cluster is twice as large for ^{8}He as it is for ^{6}He. The σ_{2n}/σ_{1n} ratio would then be the same for both projectiles, as is apparently the case. However, the reality is presumably more complicated since while the empirical spectroscopic factors for the $\langle ^8$He $| ^7$He $+ n \rangle$ and $\langle ^6$He $| ^5$He $+ n \rangle$ overlaps do differ by approximately a factor of 2 [23], those for the $\langle ^8$He $| ^6$He $+ 2n \rangle$ and $\langle ^6$He $| ^4$He $+ 2n \rangle$ are about the same [23]. The apparent similarity of the σ_{2n}/σ_{1n} ratios for the two isotopes could possibly be explained by an increased importance of two-step neutron stripping for ^{8}He, but this remains to be confirmed. Also, the uncertainties in the transfer cross sections are at present still too large to draw firm conclusions. Nevertheless, it is clear that for ^{8}He incident on a ^{208}Pb target the breakup cross section must be considerably smaller than the values obtained for the ^{6}He $+ ^{206}$Pb (151 mb at 18 MeV, calculated [21]) or ^{6}He $+ ^{209}$Bi (205 ± 65 mb

at 22.5 MeV, measured [20]) systems. Definitive conclusions will have to await the availability of more intense ^{8}He beams than those currently available to allow multiple α or ^{6}He plus neutron coincidence measurements although, as this work has shown, much can be inferred from inclusive charged-particle measurements by making physically reasonable assumptions.

[1] G. Marquínez-Durán, I. Martel, A. M. Sánchez-Benítez, L. Acosta, R. Berjillos, J. Dueñas, K. Rusek, N. Keeley, M. A. G. Alvarez, M. J. G. Borge *et al.*, Phys. Rev. C **94**, 064618 (2016).

[2] Z. Podolyák, P. M Walker, H. Mach, G. de France, G. Sletten, F. Azaiez, J. M. Casandjian, B. Cederwall, D. M. Cullen, Zs. Dombrádi *et al.*, Nucl. Instrum. Methods Phys. Res. A **511**, 354 (2003).

[3] A. Lemasson, A. Navin, M. Rejmund, N. Keeley, V. Zelevinsky, S. Bhattacharyya, A. Shrivastava, D. Bazin, D. Beaumel, Y. Blumenfeld *et al.*, Phys. Lett. B **697**, 454 (2011).

[4] A. Lemasson, A. Shrivastava, A. Navin, M. Rejmund, N. Keeley, V. Zelevinsky, S. Bhattacharyya, A. Chatterjee, G. de France, B. Jacquot *et al.*, Phys. Rev. Lett. **103**, 232701 (2009).

[5] G. Marquínez-Durán, L. Acosta, R. Berjillos, J. A. Dueñas, J. A. Labrador, K. Rusek, A. M. Sánchez-Benítez, and I. Martel, Nucl. Instrum. Methods Phys. Res. A **755**, 69 (2014).

[6] G. Marquínez-Durán, N. Keeley, K. W. Kemper, R. S. Mackintosh, I. Martel, K. Rusek, and A. M. Sánchez-Benítez, Phys. Rev. C **95**, 024602 (2017).

[7] D. M. Brink, Phys. Lett. B **40**, 37 (1972).

[8] J. L. C. Ford, Jr., K. S. Toth, G. R. Satchler, D. C. Hensley, L. W. Owen, R. M. DeVries, R. M. Gaedke, P. J. Riley, and S. T. Thornton, Phys. Rev. C **10**, 1429 (1974).

[9] C. Olmer, M. Mermaz, M. Buenerd, C. K. Gelbke, D. L. Hendrie, J. Mahoney, D. K. Scott, M. H. Macfarlane, and S. C. Pieper, Phys. Rev. C **18**, 205 (1978).

[10] K. Rusek, N. Alamanos, N. Keeley, V. Lapoux, and A. Pakou, Phys. Rev. C **70**, 014603 (2004).

[11] P. A. Assimakopoulos, Comput. Phys. Commun. **10**, 385 (1975).

[12] I. J. Thompson, Comput. Phys. Rep. **7**, 167 (1988).

[13] N. Keeley, F. Skaza, V. Lapoux, N. Alamanos, F. Auger, D. Beaumel, E. Becheva, Y. Blumenfeld, F. Delaunay, A. Drouart *et al.*, Phys. Lett. B **646**, 222 (2007).

[14] D. G. Kovar, N. Stein, and C. K. Bockelman, Nucl. Phys. A **231**, 266 (1974).

[15] J. Cook, Nucl. Phys. A **388**, 153 (1982).

[16] A. M. Sánchez-Benítez, D. Escrig, M. A. G. Álvarez, M. V. Andrés, C. Angulo, M. J. G. Borge, J. Cabrera, S. Cherubini, P. Demaret, J. M. Espino *et al.*, Nucl. Phys. A **803**, 30 (2008).

[17] M. Mazzocco, D. Torresi, D. Pierroutsakou, N. Keeley, L. Acosta, A. Boiano, C. Boiano, T. Glodariu, A. Guglielmetti, M. La Commara *et al.*, Phys. Rev. C **92**, 024615 (2015).

[18] J. P. Bychowski, P. A. DeYoung, B. B. Hilldore, J. D. Hinnefeld, A. Vida, F. D. Becchetti, J. Lupton, T. W. O'Donnell, J. J. Kolata, G. Rogachev *et al.*, Phys. Lett. B **596**, 26 (2004).

[19] P. A. DeYoung, P. J. Mears, J. J. Kolata, E. F. Aguilera, F. D. Becchetti, Y. Chen, M. Cloughesy, H. Griffin, C. Guess, J. D. Hinnefeld *et al.*, Phys. Rev. C **71**, 051601(R) (2005).

[20] J. J. Kolata, H. Amro, F. D. Becchetti, J. A. Brown, P. A. DeYoung, M. Hencheck, J. D. Hinnefeld, G. F. Peaslee, A. L. Fritsch, C. Hall *et al.*, Phys. Rev. C **75**, 031302(R) (2007).

[21] Ł. Standyło, L. Acosta, C. Angulo, R. Berjillos, J. A. Duenas, M. S. Golovkov, N. Keeley, T. Keutgen, I. Martel, M. Mazzocco *et al.*, Phys. Rev. C **87**, 064603 (2013).

[22] A. V. Nesterov, V. S. Vasilevsky, and O. F. Chernov, Phys. At. Nucl. **64**, 1409 (2001).

[23] N. Keeley, N. Alamanos, K. W. Kemper, and K. Rusek, Prog. Part. Nucl. Phys. **63**, 396 (2009).